Published in final edited form as:
J Biomed Opt. 2009 ; 14(3): 030501. doi:10.1117/1.3127202.

Imaging of Glioma Tumor with Endogneous Fluoresence Tomography

Dax S. Kepshire[1], **Summer L. Gibbs-Strauss**[1], **Julia A. O'Hara**[1,4], **Michael Hutchins**[2], **Niculae Mincu**[2], **Frederic Leblond**[1], **Mario Khayat**[2], **Hamid Dehghani**[3], **Subhadra Srinivasan**[1], and **Brian W. Pogue**[1]

[1]Thayer School of Engineering, Dartmouth College, Hanover NH 03755

[2]ART Advanced Research Technologies Inc, Saint-Laurent, Quebec, Canada H4S 2A4

[3]School of Physics, University of Exeter, Stocker Road, Exeter, EX4 4QL, UK

[4]Department of Diagnostic Radiology, Dartmouth Medical School, Hanover NH 03755

Abstract

Tomographic imaging of a glioma tumor with endogenous fluorescence is demonstrated using a non-contact single photon counting fan-beam acquisition system interfaced with microCT imaging. The fluorescence from protoporphyrin IX was found to be detectable, and allowed imaging of the tumor from within the cranium, even though the tumor presence was not visible in the microCT image. The combination of single photon counting detection and normalized fluorescence to transmission detection at each channel allowed robust imaging of the signal. This demonstrated use of endogenous fluorescence stimulation from aminolevulinic acid, provides the first in vivo demonstration of deep tissue tomographic imaging with protoporphyrin IX.

Fluorescence tomography provides a tool for pre-clinical molecular contrast agent assessment in oncology(1-4). Systems have advanced in complexity to where non-contact imaging(5), automated boundary recovery (6) and sophisticated internal tissue shapes can be included in the recovered images. The translation of this work to humans will require molecular contrast agents which are amenable to regulatory approval, and maintain tumor specificity in humans, where often non-specific uptake of molecular imaging agents can decrease their utility. In this study, a new fluorescence tomography system coupled to microCT (7) was used to illustrate diagnostic detection of orthotopic glioma tumors that were not apparent in the microCT images, using endogenous fluorescent contrast from protoporphyrin IX (PpIX).

Glioma tumors provide significant endogenous fluorescence from PpIX (8-11) and this is enhanced when the subject imaged has been administered aminolevulinic acid. The endogenous production process if PpIX is known to stem from the administered ALA bypassing the regulatory inhibition of ALA synthase, allowing the heme synthesis pathway to proceed uninhibited. Since there is limited supply of iron in the body, this process produces overabundance of PpIX rather than heme, and many tumors have been shown to have high yields of PpIX. Clinical trials with PpIX fluorescence guided resection of tumors has shown significant promise(12), and yet deep tissue imaging with PpIX fluorescence has not been exploited in clinical use. Early studies have shown that detection of these tumors with PpIX is feasible (13,14), but no tomographic imaging has been used. This limitation in development has largely been caused by problems in wavelength filtering and low signal intensity, as well as background fluorescence from the skin limiting sensitivity to deeper structures. In the system developed and used here, this feasibility is demonstrated by imaging a human xenograft glioma model.

To solve the sensitivity problem, and study the ability to diagnostically image PpIX in vivo, time-correlated single photon counting was used in the fluorescence tomography system which provides maximum sensitivity. Figure 1 (a) shows the system designed to match up with a microCT, allowing both x-ray structural and optical functional imaging sequentially. Lens coupled detection of signals are acquired from the mouse using 5 time-resolved photomultiplier tubes (H7422P-50, Hamamatsu, Japan) with single photon counting electronics (SPC-134 modules, Becker and Hickl GmbH, Germany). The system has fan-beam transmission geometry similar to a standard CT scanner, with single source delivery of a 1 mW pulsed diode laser light at 635 nm, collimated to a 1 mm effective area on the animal. The 5 detection lenses were arranged in an arc, each with 22.5° angular separation, centered directly on the opposite side of the animal with long working distance pickup (7), allowing non-contact measurement of the diffuse light through the animal. The diffuse intensity signals collected at each of the 5 channels were then translated via 400 μm fibers, and split using beamsplitters to be directed toward the fluorescence (95%) and transmission (5%) channel detectors. A 650 long-pass filter was used in the fluorescence channels to isolate the signal, and in the transmitted intensity signals a neutral density filter (2 OD) was used to attenuate the signals. This latter filtering was necessary to ensure the fluorescence and transmission intensity signals fell within the same dynamic range, allowing a single 1 second acquisition for each detector. Scans were then performed by rotating the fan-beam around the specimen to 32 locations. A GE eXplore Locus SP scanner (GE Healthcare, London ON Canada) that incorporated a detector with 94 micron pixel resolution, a 80kV peak voltage, and a tube current of 450 μAs, was used in acquiring the microCT data, as displayed in Figure 3. In this example, since soft tissue was being imaged, the CT data was largely used to image the exterior of the animal, although in future studies it could be used to isolate the cranium region as well.

Calibration of the fluorescence tomography system was carried out with standard tissue-simulating epoxy resin phantoms with tissue-like scatter and absorption coefficients. The details of the calibration procedure have been reported previously (7,15-17) and a single phantom is shown here to illustrate the type of data, as shown in Figure 1(b). The phantom contained an 8mm liquid inclusion filled with 1μg/ml PpIX. This concentration is similar to that seen in malignant gliomas (12-14). Experimental data sets were then calibrated into the fluorescence to transmission signal ratio at each detection location and then the signal was scaled such that the average ratio matched that of the model (16,18). In Figure 1 (c), the calibrated dataset used to generate this image is shown along with the reconstructed fit, illustrating convergence of this dataset with NIRFAST finite-element-based non-linear reconstruction (17,19). The system noise was determined at SNR of 1.1% in the raw fluorescence-to-transmission data, as assessed by repeated samplings of a stable signal. This level is acceptable for reconstruction of the fluorescence yield, and consistent with levels seen in previous diffuse tomography systems. The concentration of PpIX in the phantom was increased over ranges expected in tissue, and the images were reconstructed. The value in the region of interest was extracted and plotted in Figure 2.

The animal model was the U251 xenograft glioma line, grown in the laboratory for ongoing detection studies and published extensively (13,14) and is known to have high PpIX levels. The experimental plan was approved by the Institutional Animal Care and Use Committee. Briefly 10^6 cells were stereotactically implanted into the brain in 10 μL of PBS through a Hamilton syringe, through a 1 mm hole in the skull. Tumors were implanted 2mm deep into the brain with injection over 5 minutes. The tumor was incubated for 14 days and imaged *in vivo* with contrast magnetic resonance to assess size and location. Figure 3(a) shows a gadolinium-enhanced T1 weighted image of the tumor. A microCT dataset was then acquired and an exposure time of 100 ms was used, with 3 repeated measurements at each of the 400 gantry angles, for a total acquisition time of 11 minutes. The mouse bed to hold the animal was the original microCT carbon fiber bed supplied by GE, with slots cut to allow optical

measurement laterally across the cranium. After CT imaging, the animal and bed were positioned in the fluorescence tomography system and a pre-ALA-injection dataset was acquired with 64 angles using integration time of 4 seconds per angle, with a 10 minute total acquisition. Following administration of ALA and incubation over 1 hr, the animal was re-imaged using the fluorescence scanner, and a post contrast dataset was generated. The external boundary representing the cranium in the 2-D region of interest was then segmented and used to create a finite element mesh (20) for fluorescence tomography reconstruction. The contour information from the microCT allowed calculation of source and detector locations in an automated fashion.

The peak Q-band excitation for PpIX is known to be at 635 nm wavelength excitation with a molar absorption coefficient near 10^4 M^{-1} cm^{-1}, which is why the system designed here used this laser for excitation. The peak of the emission is near 640 nm, which would be challenging to detect with 635 nm excitation because of the problems in filtering. However it has a long emission tail with a second peak out near 700 nm, allowing effective fluorescence detection with the 650 nm long pass filters designed into the system. The fluorescence quantum yield of this compound is estimated to be near 0.5% (16). The fluorescence to transmission ratio data was calibrated as in the phantom study and reconstructed to create the image in Figure 3 (b). This was then superimposed on the microCT image, as shown in Figure 3 (c), to create a hybrid structural functional image of the endogenous fluorescence contrast. The microCT image did not show any evidence of the tumor, and prior studies with injected contrast did not show any promise of visualizing this intracranial tumor, due to the inherent soft tissue contrast limitations of microCT imaging. Recovery of the spatial distribution of fluorescence yield was robust however, and indicates an effective Pp-IX concentration near 10 μg/ml. This value is based upon the phantom calibration curve, although exact quantitative recovery of tomographic images must be interpreted carefully with validation by similar sized objects in similar positions to the true case.

In summary, this paper presents initial evidence that non-invasive tomography of tumors with PpIX fluorescence can be achieved, using non-contact near-infrared signal measurement. The most important factor in being able to achieve this imaging was the use of single photon counting, which allowed imaging through deep tissue in a reasonable timeframe. Another important factor was the use of ratio data of the fluorescence to transmission signals, acquired simultaneously, because this ratio is resistant to many calibration errors, distance inaccuracies or tissue heterogeneity. The exterior boundary from microCT provided higher accuracy in localization of the reconstructed volume, and so the combination of microCT and fluorescence tomography was beneficial. Further use of interior structures from microCT imaging could also enhance the localization and quantitative estimation of fluorescence *in vivo*.

Acknowledgments

This work was funded by NIH Research Grant R01CA120368 and ART Inc.

References

1. Ntziachristos V, Tung CH, Bremer C, Weissleder R. Fluorescence molecular tomography resolves protease activity in vivo. Nature Medicine 2002;8(7):757–60.
2. Choi HK, Yessayan D, Choi HJ, Schellenberger E, Bogdanov A, Josephson L, Weissleder R, Ntziachristos V. Quantitative analysis of chemotherapeutic effects in tumors using in vivo staining and correlative histology. Cellular Oncology 2005;27(3):183–90. [PubMed: 16037639]
3. Ntziachristos V, Schellenberger EA, Ripoll J, Yessayan D, Graves E, Bogdanov A Jr. Josephson L, Weissleder R. Visualization of antitumor treatment by means of fluorescence molecular tomography with an annexin V-Cy5.5 conjugate. Proceedings of the National Academy of Sciences of the United States of America 2004;101(33):12294–9. [PubMed: 15304657]

4. Ntziachristos V. Fluorescence molecular imaging. Annual Review of Biomedical Engineering 2006;8:1–33.
5. Deliolanis N, Lasser T, Hyde D, Soubret A, Ripoll J, Ntziachristos V. Free-space fluorescence molecular tomography utilizing 360 degrees geometry projections. Optics Letters 2007;32(4):382–4. [PubMed: 17356660]
6. Meyer H, Garofalakis A, Zacharakis G, Psycharakis S, Mamalaki C, Kioussis D, Economou EN, Ntziachristos V, Ripoll J. Noncontact optical imaging in mice with full angular coverage and automatic surface extraction. Applied Optics 2007;46(17):3617–27. [PubMed: 17514324]
7. Kepshire D, Mincu N, Hutchins M, Gruber J, Dehghani H, Hypnarowski J, Leblond F, Khayat M, Pogue BW. A MicroCT guided fluorescence tomography system for small animal molecular imaging. Rev. Sci. Instr. 2009 in press.
8. Kennedy JC, Pottier RH. Endogenous protoporphyrin IX, a clinically useful photosensitizer for photodynamic therapy. J. Photochem. Photobiol. B: Biol 1992;14(4):275–92.
9. Kriegmair M, Baumgartner R, Knuechel R, Steinbach P, Ehsan A, Lumper W, Hofstadter F, Hofstetter A. Fluorescence photodetection of neoplastic urothelial lesions following intravesical instillation of 5-aminolevulinic acid. Urology 1994;44(6):836–41. [PubMed: 7985312]
10. Cubeddu R, Canti G, Taroni P, Valentini G. delta-Aminolevulinic acid induced fluorescence in tumour-bearing mice. Journal of Photochemistry & Photobiology. B - Biology 1995;30(1):23–7.
11. Marcus SL, Sobel RS, Golub AL, Carroll RL, Lundahl S, Shulman DG. Photodynamic therapy (PDT) and photodiagnosis (PD) using endogenous photosensitization induced by 5-aminolevulinic acid (ALA): current clinical and development status. J. Clin. Laser Med. Surg 1996;14(2):59–66. [PubMed: 9484077]
12. Stummer W, Pichlmeier U, Meinel T, Wiestler OD, Zanella F, Reulen H-J, A.L.-G.S. Group. Fluorescence-guided surgery with 5-aminolevulinic acid for resection of malignant glioma: a randomised controlled multicentre phase III trial. Lancet Oncology 2006;7(5):392–401. see comment. [PubMed: 16648043]
13. Gibbs-Strauss SL, O'Hara JA, Hoopes PJ, Hasan T, Pogue BW. Noninvasive Measurement of Aminolevulinic Acid-induced Protoporphyrin IX Fluorescence Allows Detection of Glioma In Vivo. J. Biomed. Optics. 2008 in press.
14. Gibbs-Strauss SL, O'Hara JA, Srinivasan S, Hoopes PJ, Hasan T, Pogue BW. Diagnostic Detection of Diffuse Glioma Tumors In Vivo with Molecular Fluorescence Transmission from Endogenous Proteins. Medical Physics. 2008 in press.
15. Ntziachristos V, Ma XH, Chance B. Time-correlated single photon counting imager for simultaneous magnetic resonance and near-infrared mammography. Review of Scientific Instruments 1998;69(12): 4221–4233.
16. Davis SC, Springett R, Leussler C, Mazurkewitz P, Tuttle S, Gibbs-Strauss SL, Dehghani H, Pogue BW, Paulsen KD. Magnetic resonance-coupled fluorescence tomography scanner for molecular imaging of small animals and human breasts. Rev. Sci. Instr 2008;79:064302.
17. Kepshire DS, Davis SC, Dehghani H, Paulsen KD, Pogue BW. Subsurface diffuse optical tomography can localize absorber and fluorescent objects but recovered image sensitivity is nonlinear with depth. Applied Optics 2007;46(10):1669–78. [PubMed: 17356609]
18. Ntziachristos V, Turner G, Dunham J, Windsor S, Soubret A, Ripoll J, Shih HA. Planar fluorescence imaging using normalized data. Journal of Biomedical Optics 2005;10(6):064007. [PubMed: 16409072]
19. Davis SC, Dehghani H, Wang J, Jiang S, Pogue BW, Paulsen KD. Image guided diffuse optical fluorescence tomography implemented with Laplacian-type regularization. Optics Express 2007;15 (7):4066–4082. [PubMed: 19532650]
20. Dehghani H, Eames ME, Yalavarthy PK, Davis SC, Srinivasan S, Carpenter CM, Pogue BW, Paulsen KD. Near infrared optical tomography using NIRFAST: Algorithm for numerical model and image reconstruction. Comm. Num. Meth. Eng. 2008 published online.

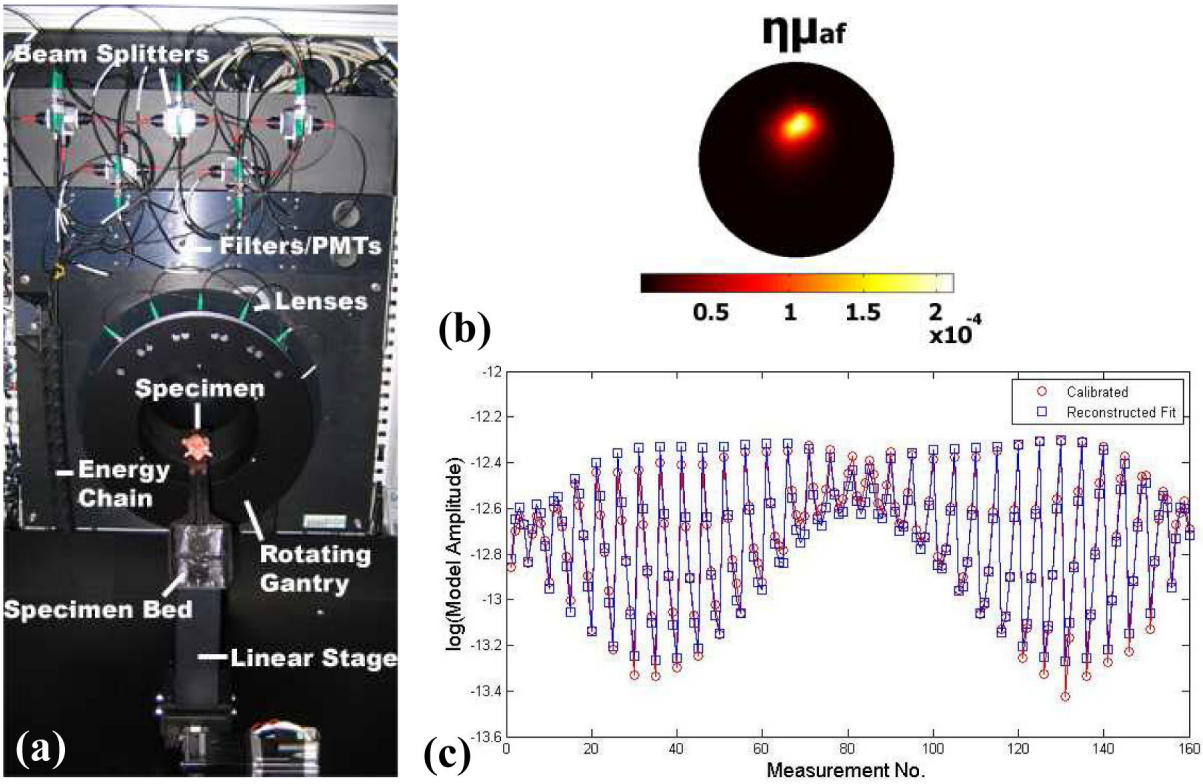

Figure 1.

The fluorescence tomography system photograph is shown in (a), with the main components labeled. A tomography dataset as measured through a tissue phantom, and (b) the reconstructed image data is overlayed on this, and in (c) the recovered image from the phantom is shown.

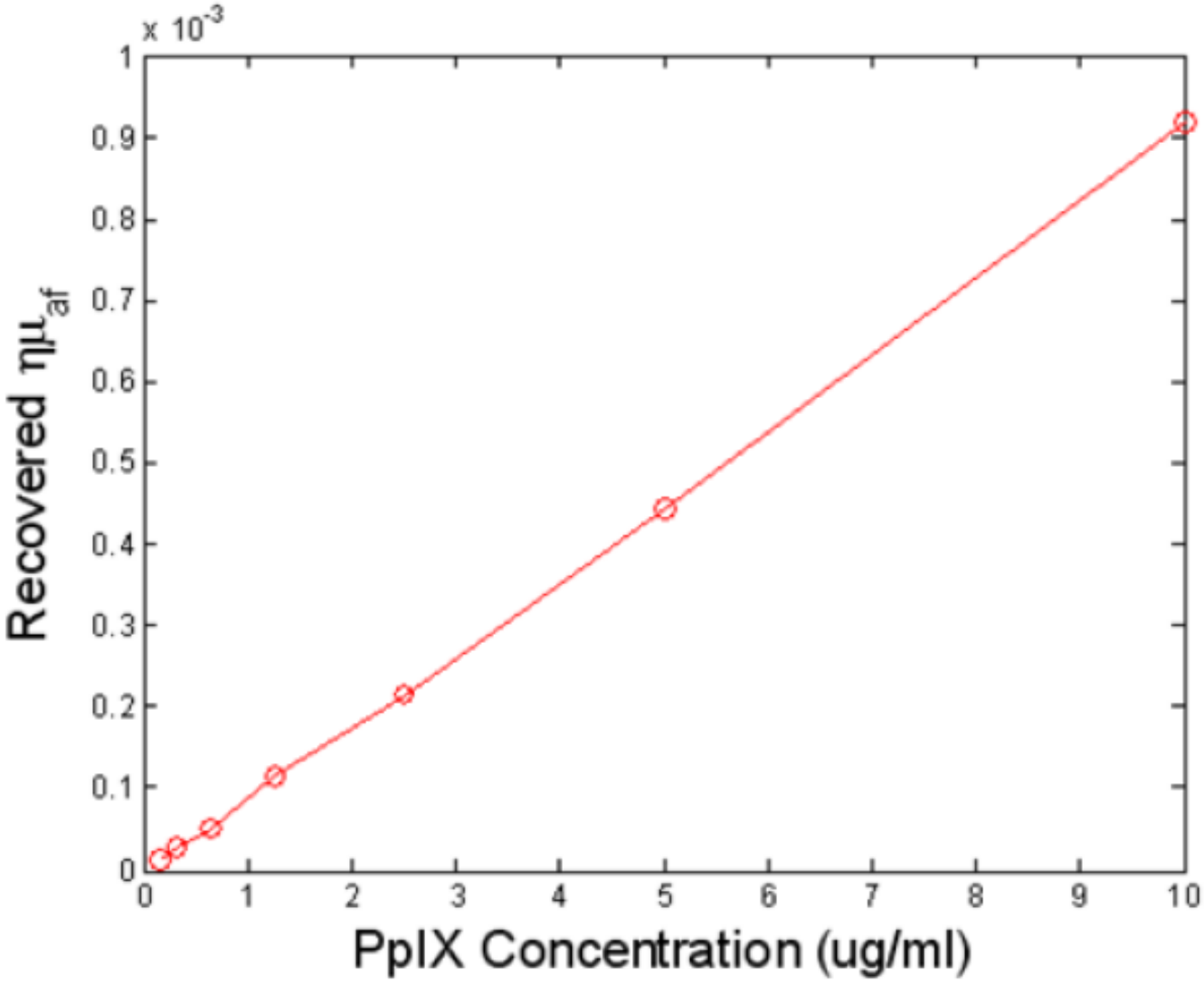

Figure 2.
The reconstructed quantum yield multiplied by the fluorophore absorption coefficient is shown within the region of the phantom, for a range of increasing PpIX concentrations. The linearity of the recovery provides a reliable way to calibrate the concentration from within tomographic images.

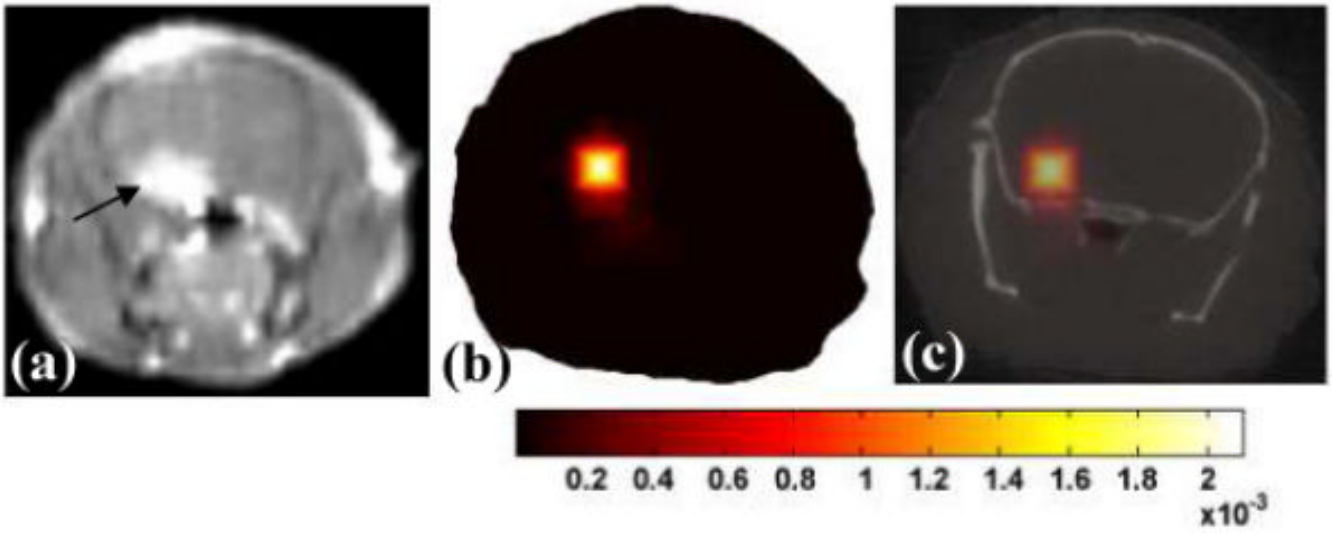

Figure 3.
Image of the rodent glioma tumor, as viewed by contrast magnetic resonance imaging (a), and the fluorescence tomography image of PpIX in (b), and the overlay of this image onto the MicroCT image of the cranium slice (c).